Efficient Acrylic Acid Production through Bio Lactic Acid Dehydration over NaY Zeolite Modified by Alkali Phosphates

Junfeng Zhang,[†] Yuling Zhao,[†] Min Pan,[†] Xinzhen Feng,[†] Weijie Ji,[*,†] and Chak-Tong Au[*,‡]

[†]Key Laboratory of Mesoscopic Chemistry, MOE, School of Chemistry and Chemical Engineering, Nanjing University, Nanjing 210093, China

[‡]Department of Chemistry, Hong Kong Baptist University, Kowloon Tong, Hong Kong

ABSTRACT: Alkali phosphates-modified NaY zeolites were developed as catalysts for efficient conversion of lactic acid to acrylic acid. The catalytic performance was optimized in terms of the type and loading of alkali phosphates, reaction temperature, liquid hourly space velocity, and lactic acid concentration. A high acrylic acid yield of 58.4% was achieved at 340 °C over 14 wt % Na_2HPO_4/NaY. The physicochemical properties of the catalysts were investigated by various techniques including NH_3-TPD, pyridine adsorption-FTIR, Raman, and MAS ^{31}P NMR. Introduction of alkali phosphates to NaY zeolite results in a decline of surface acidity. The results of FTIR, Raman, and MAS ^{31}P NMR investigations on the fresh and used catalysts suggest that sodium phosphate is largely transformed to sodium lactate during the reaction. The phosphates and the in situ generated sodium lactate function as highly active species for the target reaction.

**KEYWORDS:** alkali phosphate, NaY, dehydration, lactic acid, acrylic acid
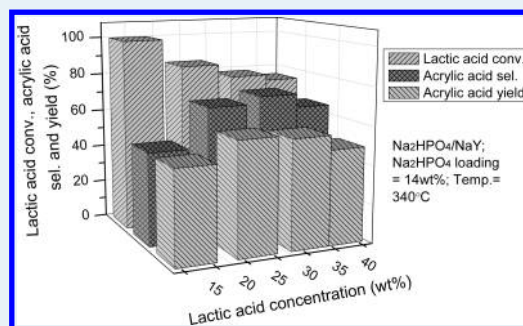
1. INTRODUCTION

Acrylic acid (AA) is an unsaturated organic compound widely used in the manufacture of paint additives, adhesive, textile and leather treating agents.[1,2] At present, AA is industrially produced by the partial oxidation of propylene through a two-step process. In recent years, the partial oxidation of propane to AA through a one-step process has drawn much attention.[3−8] Despite that multicomponent metal oxides are catalytically active for one-step oxidation, they are sensitive to preparation parameters and not efficient enough for practical application. Furthermore, both propylene and propane are from non-sustainable sources in the petrochemical industry. With the ever rising demand for petroleum, it is getting costly to use propylene as feedstock. The motivation of the present work is to find a green and environment-friendly approach for the production of AA from renewable lactic acid (LA).[9]

With different functional groups, LA has many industrial applications. The production of LA through biomass (such as glucose and starch) fermentation is a mature process.[10−12] As shown in Scheme 1, AA can be generated from LA together with the formation of 2,3-pentanedione, acetaldehyde, and so forth.[13] Therefore, the aim of the present study is to enhance AA selectivity along the dehydration path. The conversion of LA to AA and other products over catalysts of silica-aluminum salts (sulfate, nitrate, phosphate, etc.) and mixtures of inorganic salts was patented by Holmen.[14] Paparizos et al.[15] patented aluminum phosphate that was treated with an aqueous solution of inorganic base and subsequently calcined at a temperature in the 300−650 °C

Scheme 1. Reaction Pathways for LA Conversion
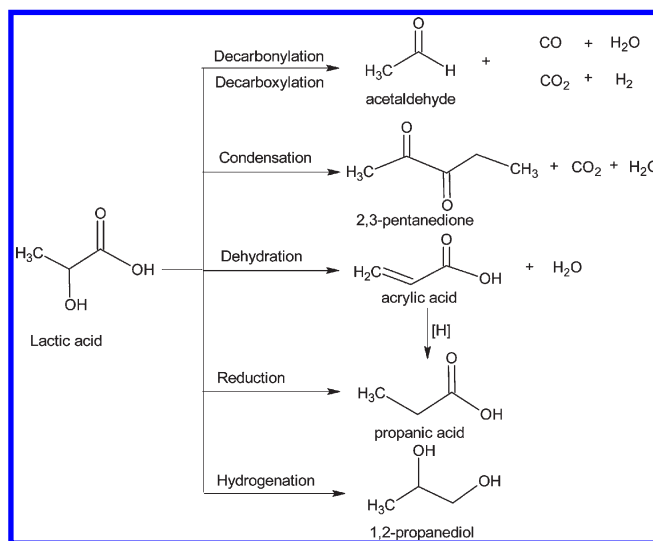
range; they claimed an AA yield of 43% at 340 °C. Sawicki[16] investigated the silica/alumina-supported Na_2HPO_4 system

(using NaHCO$_3$ as pH adjuster), and claimed an AA yield >50% at 350 °C. Miller et al.[17−23] studied the reaction mechanism of LA conversion over salts of alkali metals that were supported on silica−alumina of low specific surface area. They reported that alkali lactates were formed because of LA interaction with the catalysts, and concluded that the formation of alkali lactates is crucial for AA formation.

The use of phosphates as catalysts for alcohol dehydration was systematically studied by Monma.[24] Daniel[25] and Watkins[26] reported that phosphate salts could stabilize the carboxyl group and suppress side reactions. Mok et al.[27] and Lira and McCrackin[28] studied the generation of AA from LA under severe reaction conditions of supercritical water and observed AA yields that were above 50%. It is worth pointing out that another process was reported for AA production from LA in the 1940s: LA was first converted to 2-acetoxy propionic acid through interaction with acetic acid, and AA was liberated from the ester.[29−31] The process, however, has the disadvantage of high acetic acid consumption.

It is well-known that Y-type zeolite can be used as catalyst for alcohol dehydration.[32,33] Wang et al.[34] and Sun et al.[35] reported, respectively, the modification of NaY with KNO$_3$ and with lanthanum oxide that resulted in AA yield of 49.4−56.3%. Using silica-supported sodium dihydrogen phosphate as catalyst, Zhang et al.[36] achieved "methyl acrylate (MA) + AA" selectivity of about 50%. The results of catalyst characterization suggested that the amount of terminal POH groups diminishes at high Na/P ratios, and the enhancement of (MA+AA) selectivity is a consequence of decline in catalyst acidity.

In the present study, we focused on the modification of NaY with phosphate salts for the catalytic dehydration of LA to AA, paying particular attention to the optimization of catalytic performance. Through the control of reaction parameters as well as the type and loading of phosphate salts, we aimed to understand the physicochemical characteristics of the catalysts and to establish a relationship between catalyst structure and performance.

2. EXPERIMENTAL SECTION

2.1. Materials. LA (analytic grade) was obtained from Sinopharm Chemical Reagent Co., and deionized water was used for its dilution. The alkali phosphates (NaH$_2$PO$_4$, Na$_2$HPO$_4$, K$_2$HPO$_4$, and Na$_3$PO$_4$) and nitrates, together with hydroquinone were obtained from Sigma-Aldrich. NaY zeolite (SiO$_2$/Al$_2$O$_3$ = 2.5) was purchased from the Nankai University (China). Hydroquinone (in appropriate amount) was used as polymerization inhibitor.

2.2. Catalyst Preparation. To ensure complete Na$^+$ exchange, the purchased NaY zeolite was treated in 1 mol/L NaNO$_3$ aqueous solution. The treated NaY zeolite was then impregnated with a selected phosphate. For example, 2.5 g of treated NaY was added into 25 mL aqueous solution of a desired phosphate of a particular concentration (corresponding to a desired loading). The mixture was stirred at 40 °C for 4 h, and the resulting slurry was subject to slow evaporation (in a rotary evaporator) at 60 °C until dryness. The obtained material was further dried at 120 °C overnight in an oven, and then pressed and crushed into particles of 40−60 mesh.

2.3. Catalyst Evaluation. The evaluation of catalyst activity was carried out in an upright fixed-bed quartz reactor that was 8 mm in inner diameter and 500 mm in length. The reaction was
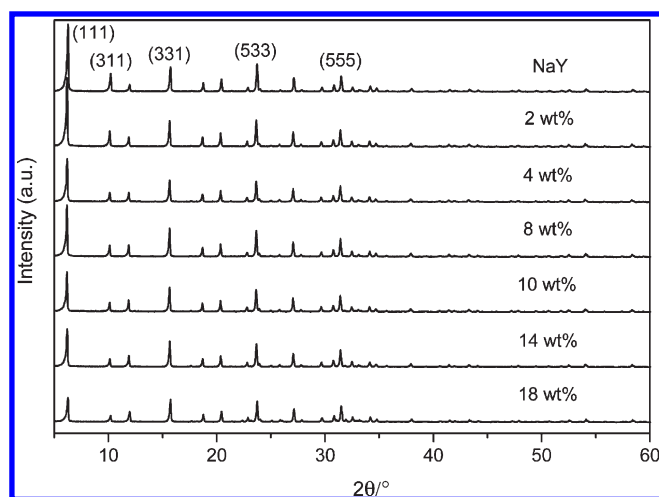

Figure 1. Wide-angle XRD patterns of NaY and 2−18 wt % Na$_2$HPO$_4$-modified NaY catalysts.

operated at atmospheric pressure. A 1.5 g portion of catalyst was charged into the reactor, and the space above the catalyst bed was filled with quartz chips to ensure preheating of the in-coming LA-containing liquid. Before introduction of the feedstock, the sample was heated up in a flow of pure N$_2$ (30 mL/min) to a desired temperature at a rate of 10 °C/min and kept at this temperature for 3 h. Then a flow of LA liquid (3−8 mL/min) was introduced, and the products were collected at a cold trap. The analysis of the collected species was conducted using a gas chromatograph equipped with FID and HP-FFAP capillary column (0.32 mm ×25 m), and valeric acid was adopted as internal standard. The amount of CO$_x$ (CO and CO$_2$) was estimated based on the yield of acetaldehyde and 2,3-pentanedione. Similar to the work of Zhang et al.,[37] LA conversion (X$_L$), yield (Y$_i$) and selectivity (S$_i$) of component "i" are defined as eqs 1−3.

$$X_L = \frac{(n_{0,L} - n_L)}{n_{0,L}} \times 100\% \qquad (1)$$

$$Y_i = \frac{n_i}{n_{0,L}} \times 100\% \qquad (2)$$

$$S_i = \frac{Y_i}{X_L} \times 100\% \qquad (3)$$

Where $n_{0,L}$ is the molar quantity of LA fed into the reactor, n_L is the molar quantity of LA in the effluent, and n_i is the mole quantity of LA equated from the i component of product.

2.4. Catalyst Characterization. Powder X-ray diffraction measurement was conducted on a Shimadzu XRD-6000 diffractometer operated at 40 kV and 40 mA with Cu-K$_a$ radiation. Phosphorus content was determined by X-ray fluorescence spectroscopy (ARL-9800).

Ammonia temperature-programmed desorption (NH$_3$-TPD) was carried out to measure the surface acidity of catalyst. First, 0.1 g of catalyst was treated in flowing Ar (30 mL/min) at 400 °C for 1 h, and then cooled to 100 °C in the Ar flow. After that the catalyst was exposed to a flow of ammonia (20 mL/min) for 60 min, and it was purged with He (30 mL/min) for 60 min. Finally, NH$_3$-TPD was carried out in He at a heating rate of 10 °C/min within the 100−500 °C range. The signal was recorded by a thermo-conductive detector.
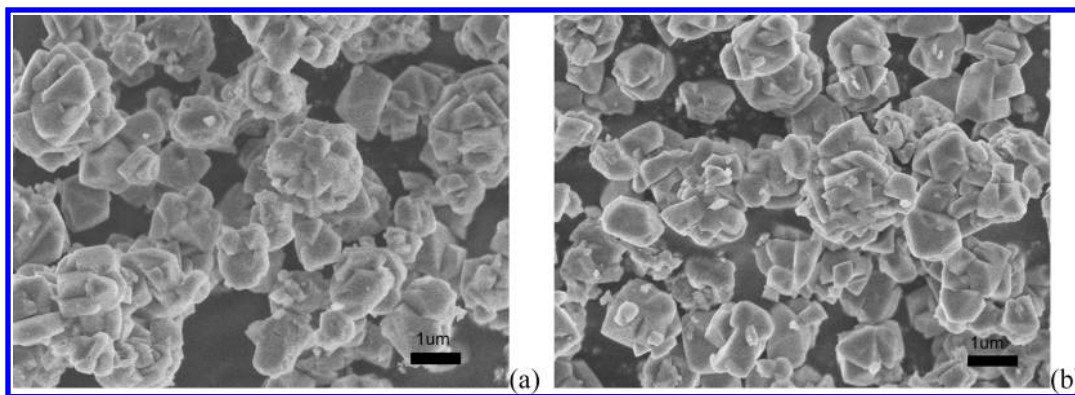
Figure 2. SEM images of the parent NaY and the impregnated NaY samples: (a) parent NaY and (b) 14 wt % Na_2HPO_4/NaY.

The FTIR spectra of pyridine adsorption were recorded in the range of $1000-4000$ cm^{-1} on a Bruker VERTEX70 spectrometer. The samples were pressed into self-supporting wafers containing 10 mg of material, and then the wafers were mounted inside a Pyrex vacuum cell and degassed at 400 °C for 2 h. Samples were allowed to cool down to room temperature (RT), and pyridine vapor was admitted into the cell and adsorption lasted for 1 h. Subsequently, the samples were heated up to a selected temperature under vacuum and cooled down to RT for spectrum recording. On the other hand, the IR spectra of the fresh and used catalysts were recorded to check the occurrence of surface phosphate transformation during the reaction. Furthermore, Raman microprobe spectroscopy (Bruker) with a laser source of 514 nm was adopted to study the fresh and used catalysts.

The specific surface areas and pore volumes of the catalysts were measured through nitrogen adsorption at 77 K using a Micrometrics ASAP 2020 instrument. Prior to adsorption, the samples were treated at 350 °C under vacuum for 8 h. The specific surface area was calculated according to the Brunauer−Emmett−Teller (BET) method, while pore volume was evaluated with the t-plot method. MAS ^{31}P NMR spectroscopy was used to distinguish the structural environment of phosphate species in the fresh and used catalysts. The measurement was conducted at 161.98 MHz on a Bruker AV-400 spectrometer equipped with a 3.2 mm MAS BB//probe, and $NH_4H_2PO_4$ was used as reference sample.

3. RESULTS AND DISCUSSION

3.1. Characterization. *3.1.1. XRD and SEM.* The wide-angle X-ray diffraction (XRD) patterns of the Na_2HPO_4-modified NaY catalysts are shown in Figure 1. With comparison to the pattern of NaY zeolite, it is deduced that the Na_2HPO_4-modified NaY catalysts essentially retain the faujasite structure, only that the intensity of (111) peaks at $2\theta = 6.2°$ decreases gradually with rise of Na_2HPO_4 loading (2−18 wt %). The results suggest that the introduction of Na_2HPO_4 to NaY zeolite has little effect on the phase structure of NaY zeolite but causes certain morphological change of the NaY particles. The Na_2HPO_4 species can hardly be detected by the XRD technique, suggesting that they are well dispersed. The scanning electron microscopy (SEM) images of the parent NaY and the impregnated NaY sample (Figure 2) indicate enhanced dispersion and also the apparent facet of primary NaY particles, suggesting that the introduction of alkali
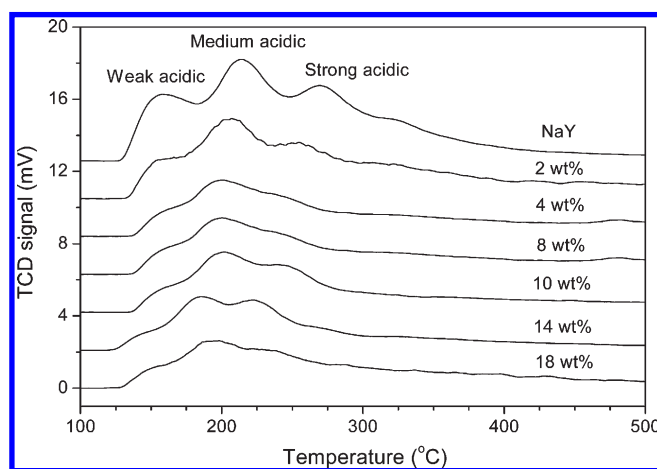

Figure 3. NH$_3$-TPD profiles of NaY and 2−18 wt % Na_2HPO_4-modified NaY catalysts.

phosphates can somehow modify the morphology of NaY crystallites.

3.1.2. NH$_3$-TPD. Shown in Figure 3 are the NH$_3$-TPD profiles recorded over the Na_2HPO_4-modified NaY of different Na_2H-PO$_4$ loadings. The unmodified NaY sample shows four desorption peaks centered at 157, 214, 270, and 323 °C. With Na_2HPO_4 addition at elevated loading, the 323 °C desorption peak disappears quickly; meanwhile, the peaks in the 150−270 °C range also diminishes. It is noted that the position of the peaks shift toward lower temperature. The observations suggest that the introduction of Na_2HPO_4 readily eliminates the sites of medium-strong acidity and reduces the density and strength of the sites of weak acidity.

3.1.3. Pyridine-Adsorption FTIR. FTIR spectra of pyridine adsorption on unmodified and Na_2HPO_4-modified NaY were collected (Figure 4) for the determination of Brønsted and Lewis acid sites.[38] All the samples have a band at 1442 cm^{-1} attributable to pyridine adsorption on Na$^+$ cation (indicative of Lewis acid sites[39]). It is noted that the characteristic band of pyridine adsorption on Brønsted acid sites at 1540 cm^{-1} is absent. This is a clear signal that the Y zeolite is fully exchanged with Na$^+$. The 1489 cm^{-1} band can be ascribed to the cocontrition of Lewis and Brønsted acid sites; in the present case, since the Brønsted acid sites are absent, the 1489 cm^{-1} band should be ascribed solely to Lewis acid sites. At higher Na_2HPO_4 loadings, the intensity of the 1442 cm^{-1} peak declines, suggesting that the
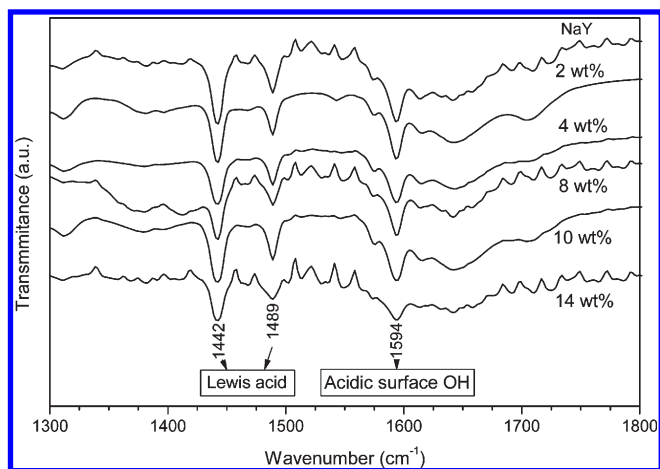
Figure 4. FTIR spectra of pyridine adsorption collected over unmodified and 2−14 wt % Na$_2$HPO$_4$-modified NaY.

Table 1. Surface Area and Pore Volume of NaY and Na$_2$HPO$_4$-Modified NaY

catalyst	BET surface area (m^2/g)	micropore volume (cm^3/g)
NaY	686	0.37
8 wt % Na$_2$HPO$_4$−NaY	584	0.25
14 wt % Na$_2$HPO$_4$−NaY	379	0.22

Na$^+$ sites associated with the framework of Y zeolite are blocked by phosphate species and the Na$^+$ cations associated with phosphate do not function as Lewis acid sites. It is noted that the band at 1594 cm^{-1} detected over the unmodified NaY also diminishes with rise of Na$_2$HPO$_4$ loading. The 1594 cm^{-1} band is plausibly due to surface OH entities that are associated with NaY. The OH species are somewhat acidic and decline in density when there is Na$_2$HPO$_4$ deposited on NaY. It is apparent that the introduction of Na$_2$HPO$_4$ to NaY does not generate any extra Brønsted or Lewis acid sites. In fact, because of the blocking of the Na$^+$ sites associated with the zeolite framework, there is reduction in the overall surface acidity, consistent with the results of the NH$_3$-TPD investigation.

3.1.4. N$_2$-Sorption Measurement. On the basis of the sorption isotherms of N$_2$ at the condensation temperature (77 K), the size and volume of the pores can be measured.[40] The BET surface areas are also obtainable for microporous samples. One should, however, realize that there are limitations of the BET method for microporous adsorbents,[41] and the reported BET surface areas can only be used as empirical values to compare the porosity of materials of the same kind.[42] From Table 1, one can see the pore structure as well as the surface area of three representative samples. It is observed that the introduction of Na$_2$HPO$_4$ to NaY results in a significant decrease in pore volume and surface area. One can envisage that with Na$_2$HPO$_4$ entities positioned at the pore mouths and/or inside the pore channels, certain amount of the NaY micropores are blocked, leading to the decrease of pore volume and also surface area. The results of sorption measurement indicate that there is good dispersion of Na$_2$HPO$_4$ species, in agreement with the XRD results. It is revealed from Figure 5 that the pore size distribution of 8 wt % was different from that observed in the parent NaY and 14% Na$_2$HPO$_4$/NaY.
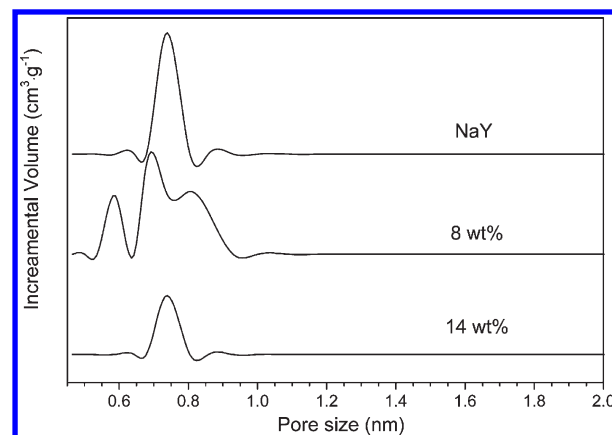

Figure 5. Pore size distribution of unmodified NaY and two selected Na$_2$HPO$_4$-modified NaY catalysts.

At 8 wt % Na$_2$HPO$_4$ loading, a larger fraction of Na$_2$HPO$_4$ entities could be inside the pore channels, causing reduction of pore diameter and generation of smaller pores. In addition, some pores of 0.9 nm seem generated, and the origin is unclear yet. Measurement of more samples with different Na$_2$HPO$_4$ loadings in 5−14 wt % range may be helpful to clarify this. At 14 wt % Na$_2$HPO$_4$ loading, larger fraction of Na$_2$HPO$_4$ species can be deposited at the pore mouths, resulting in more obvious pore blockage and pore volume reduction, while slight pore size decrease.

3.2. Catalytic Activity. *3.2.1. Effect of Phosphate Type.* The activity data collected at 350 °C with LA concentration of 34 wt % and LHSV of 2.27 h^{-1} are depicted in Table 2. All the phosphate-modified samples have the same phosphate loading of 14 wt % (corresponding to 0.986 mmol/g$_{cat}$). Over the NaY catalyst, although LA conversion is rather high (96.2%), AA yield, however, is only 24.4% because of poor AA selectivity (25.4%). It is noted that the yield of acetaldehyde over NaY is 20.7%, suggesting that the decarbonylation/decarboxylation reaction pathways depicted in Figure 1 are favored under such conditions. Over the modified NaY catalysts, there is clear suppression of the decarbonylation/decarboxylation reaction (<10% in acetaldehyde yield), and AA yield is more than 50%. Among the modified catalysts, good performance is observed over Na$_2$HPO$_4$/NaY and K$_2$HPO$_4$/NaY. It is apparent that the type of alkali metal has an impact on catalyst behavior: compared with Na$_2$HPO$_4$/NaY, K$_2$HPO$_4$/NaY is slightly less selective to AA but more selective to 2,3-pentanedione. This feature is attractive because 2,3-pentanedione is a highly value-added product used in the manufacture of fine chemicals such as perfume additives. Among the NaH$_2$PO$_4$/NaY, Na$_2$HPO$_4$/NaY, and Na$_3$PO$_4$/NaY catalysts, Na$_2$HPO$_4$/NaY is the best, showing AA selectivity of 63.2%. The results reveal that Na content has an effect on catalyst performance. It is understood that a change of Na content in phosphate can cause variation in phosphate acidity, consequently resulting in modification of surface acid−base properties. Over the serial catalysts NaH$_2$PO$_4$/NaY, Na$_2$HPO$_4$/NaY, Na$_3$PO$_4$/NaY, and K$_2$HPO$_4$/NaY, the basicity of the supported phosphates increases accordingly. On the basis of same molar loading of phosphate, the pore structure of Na$_2$HPO$_4$/NaY is plausibly rather similar to that of K$_2$HPO$_4$/NaY. From Table 2, there is a certain trend that LA conversion increases with increasing basicity of the supported phosphates while the highest AA

Table 2. Yield of Main Products, Conversion of LA, and Selectivity to AA and 2, 3-Pentanedione Observed over a Modified NaY Catalyst of 0.986 mmol/g_{cat} Phosphate Loading[a]

	catalyst	NaY	NaH$_2$PO$_4$/NaY	Na$_2$HPO$_4$/NaY	Na$_3$PO$_4$/NaY	K$_2$HPO$_4$/NaY
yield (mol %)	acetaldehyde	20.7	3.9	4.9	3.0	8.7
	2,3-pentanedione	2.6	3.1	4.4	4.6	6.9
	acetic acid	0.6	0.4	0.6	0.7	0.6
	propanic acid	3.2	1.3	1.5	1.2	1.2
	AA	24.4	42.9	51.5	51.0	51.1
conversion of LA (%)		96.2	79.4	81.5	88.3	87.0
selectivity to 2, 3-pentanedione (%)		2.7	3.9	5.4	5.2	7.9
selectivity to AA (%)		25.4	54.1	63.2	57.8	58.7

[a] Reaction temperature: 350 °C; LA concentration: 34 wt %; LA LHSV = 2.3 h^{-1}; N$_2$ carrier flow rate: 30 mL/min.

selectivity corresponds to a medium basicity of Na$_2$HPO$_4$. In other words, with similar pore structure of catalyst, the basicity of phosphate species mainly determines the AA selectivity (Na$_2$HPO$_4$/NaY vs K$_2$HPO$_4$/NaY). In the present study, different phosphates are actually compared at the optimized Na$_2$HPO$_4$ loading (see Section 3.2.2). We have not yet compared catalyst performance at a phosphate loading below 0.986 mmol/g_{cat} among different alkali metal (Na, K, Cs) phosphates, and it will be the objective of further study. According to Tam et al.,[21,22] the presence of phosphate species can stabilize the carboxyl group of LA as well.

Gunter et al.[43] reported that upon thermal treatment, Na$_2$HPO$_4$ condenses to tetra-sodium pyrophosphate, and when the Na$_2$HPO$_4$-modified catalyst is exposed to LA vapor, the transfer of a proton from LA to pyrophosphate may result in the formation of sodium lactate. Na$_3$PO$_4$ can also accept a proton from LA to generate sodium lactate and disodium phosphate, the latter is ultimately transferred to sodium lactate through proton transfer. The generation of sodium lactate is thought to be a favorable factor for LA conversion to AA and 2,3-pentanedione. The inter-transformation of phosphates and LA may reasonably explain the similarity in AA yield over the Na$_2$HPO$_4$/NaY, Na$_3$PO$_4$/NaY, and K$_2$HPO$_4$/NaY catalysts. On the other hand, NaH$_2$PO$_4$ can condense to (Na$_3$PO$_3$)$_n$ from which sodium lactate is hard to generate; this can explain why the performance of NaH$_2$PO$_4$/NaY is poor.

3.2.2. Effect of Na$_2$HPO$_4$ Loading. Through the above investigation, it is found that the Na$_2$HPO$_4$-modified NaY catalyst is the best for AA generation. It is hence selected to investigate the effect of phosphate loading on catalyst activity, and the results are shown in Figure 6. Between 0 and 0.986 mmol/g_{cat} loadings (corresponding to 0—14 wt % Na$_2$HPO$_4$), LA conversion slowly declines to around 82%, and there is a significant rise in AA selectivity. Further rise of Na$_2$HPO$_4$ loading to 1.268 mmol/g_{cat} (18 wt % Na$_2$HPO$_4$) would result in a drop of AA selectivity. The selectivity to 2,3-pentanedione does not change remarkably within the whole range of Na$_2$HPO$_4$ loading. It is clearly evidenced from Figure 6b that the formation of acetaldehyde can be significantly suppressed by increasing the loading of Na$_2$HPO$_4$. The phenomena can be related to the change of surface acidity. According to the results of NH$_3$-TPD (Figure 3) and pyridine adsorption FTIR (Figure 4) studies, there is fast decrease of surface acidity (in terms of density and strength) of catalyst upon phosphate modification. One can deduce that the decarbonylation/decarboxylation of LA to acetaldehyde is effectively restrained through phosphate modification of NaY.
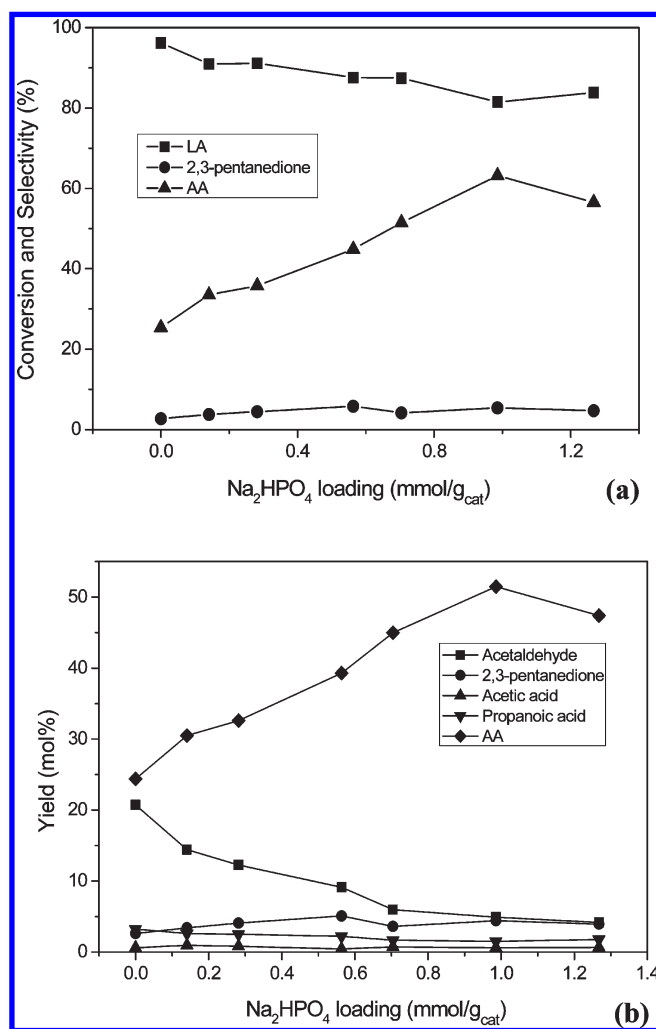

Figure 6. Effect of Na$_2$HPO$_4$ loading on (a) LA conversion as well as AA and 2,3-pentanedione selectivity, and (b) yield of major products. Reaction temperature = 350 °C, LA concentration = 34 wt %, and N$_2$ carrier flow rate = 30 mL/min.

On the other hand, a change in Na$_2$HPO$_4$ loading can alter surface area and pore structure of catalyst as revealed in Table 1 and Figure 5. Such changes may have an impact on product distribution, and this is indeed the case in terms of 2, 3-pentanedione formation. Compared to acetaldehyde, 2, 3-pentanedione is larger in size, and hence more sensitive to any change of pore size and pore volume. A slight decline in NaY pore diameter
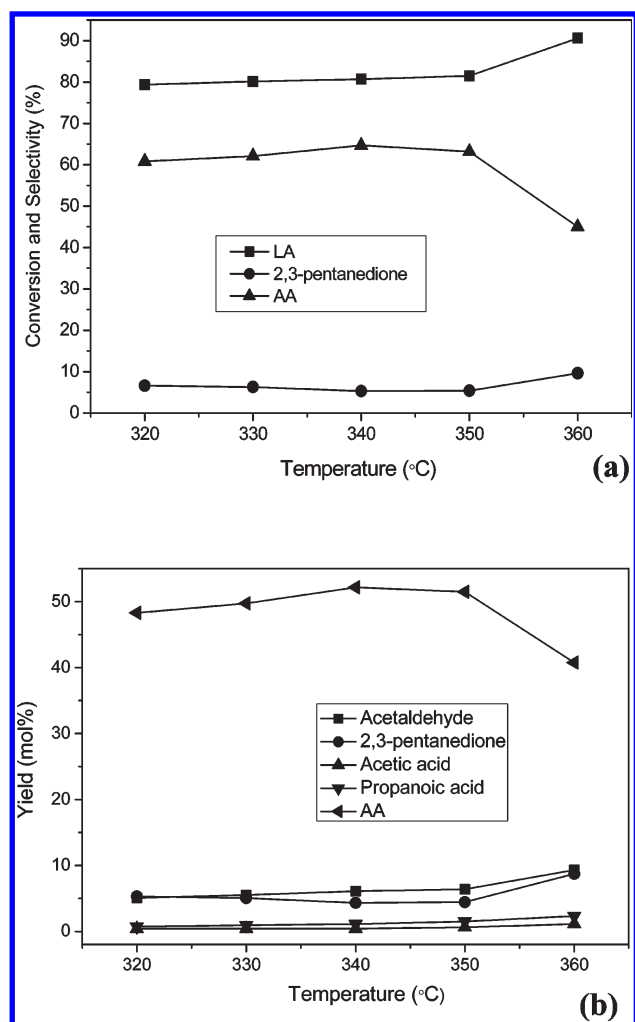
Figure 7. (a) LA conversion as well as AA and 2,3-pentanedione selectivity, and (b) yield of major products over 14 wt % Na$_2$HPO$_4$/NaY as a function of temperature. LA concentration = 34 wt % and N$_2$ carrier flow rate = 30 mL/min.

Table 3. Reaction Performance at Various LHSVs[a]

		LHSV (h^{-1})			
reaction performance		1.8	2.3	2.7	3.2
yield (mol %)	acetaldehyde	4.2	4.4	4.4	5.0
	2,3-pentanedione	4.3	4.3	4.6	4.2
	acetic acid	0.4	0.4	0.4	0.4
	propanoic acid	1.4	1.1	1.0	1.0
	AA	49.8	52.2	56.6	47.1
conversion of LA (%)		84.0	80.7	78.3	73.8
selectivity to 2, 3-pentanedione (%)		5.1	5.3	5.9	5.7
selectivity to AA (%)		59.2	64.7	72.3	63.9

[a] Catalyst: 14 wt % Na$_2$HPO$_4$/NaY; reaction temperature: 340 °C; N$_2$ carrier flow rate: 30 mL/min.

340 °C there is reduction of AA yield because side reactions such as decarboxylation/decarbonylation and condensation become favorable. It is understandable because at elevated temperatures the stability of LA carboxyl group decreases while the diffusion efficiency of 2, 3-pentanedione increases. On the other hand, the yields of propanoic and acetic acids are not significantly affected by the change of temperature. It was reported that the yield of propanoic acid is related to AA production.[23] In the present study, the hydrogenation of AA to propanoic acid appears to be limited. Nonetheless, one should bear in mind that the deposition of inactive carbon can be serious at high temperatures, bringing about the partial deactivation of catalyst.

3.2.4. Effect of Liquid Hourly Space Velocity (LHSV). The influence of LHSV on reaction performance is shown in Table 3. The reactions were conducted at 340 °C with flow rate of LA changed from 4 to 7 mL/h (corresponding LHSV = 1.8−3.2 h^{-1}). Other operation conditions such as the flow rate of N$_2$ (30 mL/min) and concentration of LA (34 wt %) were retained. It is observed from Table 3 that LA conversion decreases from 84.0% to 73.8% as LHSV increases from 1.8 to 3.2 h^{-1}. At elevated LHSV, the contact time of LA with catalyst reduces, resulting in low LA conversion. Selectivity to 2, 3-pentanedione changes little in the adopted LHSV range. However, AA selectivity increases from 59.2% to 72.3% as LHSV increases from 1.8 to 2.7 h^{-1}, and declines to 63.9% at LHSV of 3.2 h^{-1}. There is an optimal LHSV of 2.7 h^{-1} at which the highest AA yield of 56.6% can be achieved. The corresponding contact time, according to eq 4 given by Smith et al.,[44] is calculated to be 0.61 s.

$$CT = \frac{3600 \times 273 \times V_c}{22400(N_{LA} + N_c) \times T} \qquad (4)$$

Where CT is the contact time (s); V_c is the catalyst volume (mL); N_{LA} is the moles of reactant passed per hour; N_c is the moles of carrier gas per hour; and T is the reaction temperature (K).

From Table 3, one can see that the yield change of acetaldehyde, 2,3-pentanedione, acetic acid, and propanic acid within the adopted LHSV range is not drastic, plausibly because of the enhanced reaction pathway of LA dehydration. The formation of propanoic acid is known to be associated with AA concentration on catalyst surface, and a decrease in contact time would lower the AA surface concentration, and thus cause a decline of propanoic acid yield.

3.2.5. Effect of LA Concentration. LA conversion and AA yield are affected not only by LHSV but also by LA concentration

could have a "pore size" effect on selectivity to 2, 3-pentanedione, and the consequence is an improvement of 2, 3-pentanedione yield.

3.2.3. Effect of Reaction Temperature. The conversion of LA can be critically influenced by reaction temperature. The effect of reaction temperature on catalyst performance is shown in Figure 7. The reactions were carried out in the 320−360 °C range over the Na$_2$HPO$_4$/NaY catalyst with an optimized loading of 0.986 mmol/g$_{cat}$. Only a slight increase in LA conversion is observed when the reaction temperature is raised from 320 to 350 °C (Figure 7a). Further increase of temperature to 360 °C would lead to a notable increase of LA conversion. The selectivity to AA and 2,3-pentanedione essentially remain unchanged in the 320−350 °C range. At 360 °C, AA selectivity decreases considerably while 2,3-pentanedione selectivity increases. Shown in Figure 7b are the yields of the major products as a function of temperature. The yield of AA slowly increases with increasing temperature and reaches a maximum at 340 °C. There is a slight decline in AA yield at 350 °C, and the decline becomes drastic at 360 °C. The results of Figure 7b also show that the formation of acetaldehyde and 2,3-pentanedione is enhanced in the 350−360 °C range. In other words, above

Table 4. Reaction Performance at Various LA Concentrations in Solution[a]

		LA concentration in solution (wt%)			
reaction performance		40.0	34.0	25.0	15.0
yield (mol %)	acetaldehyde	2.7	4.2	5.0	11.0
	2,3-pentanedione	3.4	4.6	5.1	7.1
	acetic acid	0.3	0.4	0.5	2.2
	propanic acid	0.7	1.0	1.5	1.4
	AA	49.2	56.6	58.4	48.0
conversion of LA (%)		75.4	78.3	85.3	100.0
selectivity to 2, 3-pentanedione (%)		4.5	5.9	6.0	7.1
selectivity to AA (%)		65.3	72.3	68.5	48.0

[a] Catalyst: 14 wt % Na_2HPO_4/NaY; reaction temperature: 340 °C; N_2 carrier flow rate: 30 mL/min.
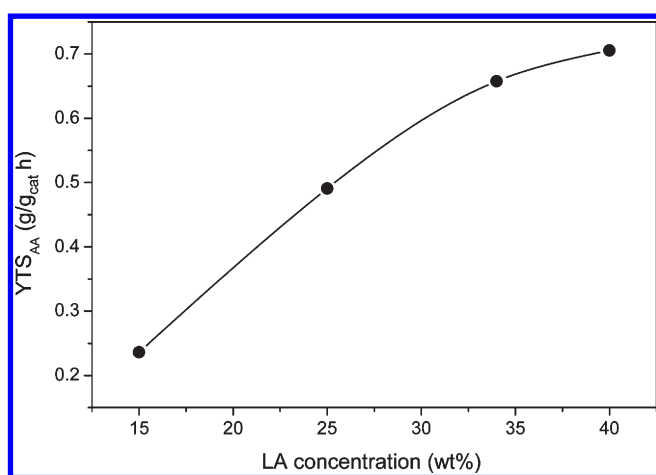

Figure 8. Time space yield of AA at different LA concentrations. Catalyst: 14 wt % Na_2HPO_4/NaY; reaction temperature: 340 °C; N_2 carrier flow rate: 30 mL/min.

in solution. Therefore, the effect of LA concentration on reaction performance was also studied, and the results are depicted in Table 4. One can observe that a decrease of LA concentration from 40 to 15 wt % can dramatically increase LA conversion from 75.4% to 100%; meanwhile AA selectivity first increases from 65.3% to 72.3% and then gradually decreases to 48.0%. One can see that there is an optimal LA concentration in solution, namely, 25 wt %, at which the highest AA yield of 58.4% can be obtained. This is in fact the highest AA yield obtained in the present study. The data shown in Table 4 indicate that a decrease of LA concentration in solution results in enhancement of the forma- tion of all other products. During the feeding of LA into the reactor, the degree of LA self-polymerization is low if the concentration of LA in the solution is low; and one would expect better efficiency of the target reaction. Furthermore, an aqueous solution of lower LA concentration contains more water (an unfavorable situation for LA dehydration). Consequently, the LA dehydration pathway is somewhat suppressed while the other reactions enhanced.

The time space yield (YTS) of AA was calculated at different LA concentrations according to eq 5:

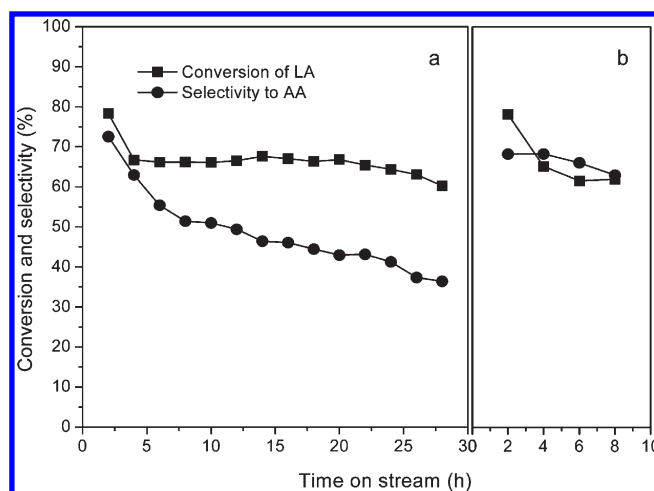$$YTS = \frac{M_{AA}}{M_{cat} \times t} \qquad (5)$$

Figure 9. Test of catalyst stability over 14 wt % Na_2HPO_4/NaY: (a) Fresh catalyst subject to a period of 28-h reaction, and (b) reactivated catalyst subject to a period of 8-h reaction. Reaction temperature = 340 °C, LA concentration = 34 wt %, LA LHSV = 2.7 h^{-1}, and N_2 carrier flow rate = 30 mL/min.

Where M_{AA} is the mass of produced AA (g); M_{cat} is the mass of catalyst (g); and t is the reaction time (h). Plotted in Figure 8 is the YTS of AA versus LA concentration. The YTS of AA increases rapidly as LA concentration increases from 15 to 34 wt %, but changes only slightly at higher LA concentration. Considering the LA conversion and output coefficient at various LA concentrations, we suggest that the optimal LA concentration is roughly 34 wt %.

3.2.6. Catalyst Stability. The stability of catalyst with time on stream was studied at 340 °C over Na_2HPO_4/NaY of 0.986 mmol/g_{cat} loading (LHSV = 2.7 h^{-1} and LA concentration = 34 wt %). From Figure 9a, one can see that LA conversion declines noticeably within the first 3 h and essentially remains unchanged afterward. The AA selectivity, however, decreases continuously in a period of 30 h. Such catalyst deactivation is thought to be a result of LA polymerization on the catalyst. To verify this point, the deactivated catalyst was treated in an air flow (30 mL/min) at 500 °C for 3 h, and the treated catalyst was tested in a second run. The results of Figure 9b suggest complete recovery of LA conversion. There is improvement of catalyst performance observed over the regenerated catalyst. It is inferred that the high temperature air-calcination of the used catalyst may bring about higher dispersion of surface phosphate species, stronger interaction between sodium lactate and NaY as well as a decrease in amount of poly lactate species, showing recovery of LA conversion and improved AA selectivity (better stabilizing effect of the well dispersed surface phosphate species on the carboxylate group of LA reactant and AA product). Nevertheless, it deserves further study to understand the details about the mechanism of catalyst deactivation and regeneration.

3.3. FTIR, Raman, and MAS ^{31}P NMR Study of the Fresh and Used Catalysts. To understand the active species that existed on the catalyst surface, the fresh and used catalysts were investigated by means of FTIR and Raman, and the results are shown in Figures 10–12. In Figure 10, the characteristic band of Na_2HPO_4 fine crystallites at 860 cm^{-1} disappears after activation at 350 °C (Na_2HPO_4 fine crystallites $\rightarrow$ well dispersed surface species). The characteristic band of $Na_4P_2O_7$ (1123 cm^{-1}) is difficult to differentiate because it overlaps with the bands of NaY.
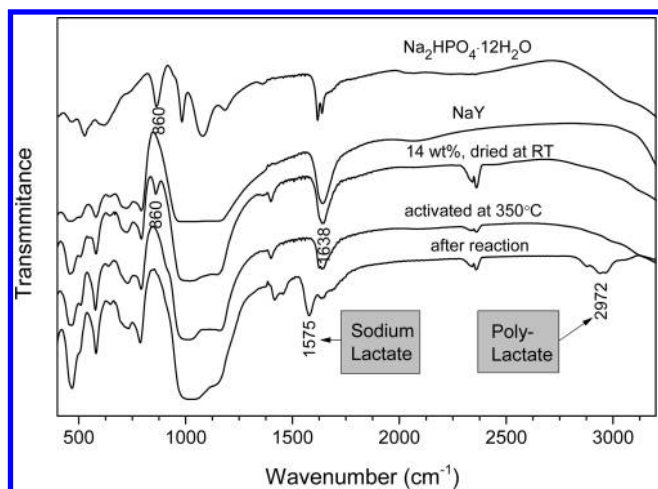
Figure 10. FTIR spectra of the dried, activated, and used catalysts together with those of reference compounds.
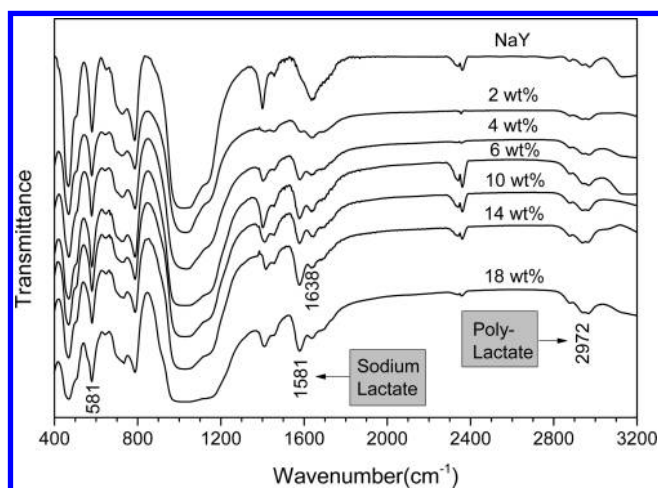

Figure 11. FTIR spectra of used catalysts of various Na_2HPO_4 loadings.

Figure 12. Raman spectra of fresh (14 wt % Na_2HPO_4/NaY) and used catalysts together with those of reference compounds.

Figure 13. ^{31}P MAS NMR spectra of fresh (14 wt % Na_2HPO_4/NaY) and used catalysts.

The band at 1638 cm^{-1} due to adsorbed H$_2$O[45] diminishes after activation. Over the used catalyst, a band at 1575 cm^{-1} ascribable to sodium lactate species is detected, indicating the formation of sodium lactate during reaction. Similar observation was reported by Gunter et al.[21] A broad band centered at 2972 cm^{-1} is also detected over the used catalyst, which is likely due to the poly lactate species. Shown in Figure 11 are the FTIR spectra of the used catalysts of different Na_2HPO_4 loadings. Note that the bands at 1581 and 2972 cm^{-1} increase in intensity at higher Na_2HPO_4 loadings. The results imply that with increasing Na_2HPO_4 loading, the formation of sodium lactate increases, and the degree of polymerization of lactate also increases.

Shown in Figure 12 are the Raman spectra of the fresh and used catalysts. Over the fresh catalyst, a broad band in the 950−1100 cm^{-1} range attributable to a mixture of Na_2HPO_4 and $Na_4P_2O_7$ species[36] is observed. In comparison with the Raman spectra of the reference compounds, one may deduce that the structures of surface Na_2HPO_4 and $Na_4P_2O_7$ species are highly distorted. The content of Na_2HPO_4 and $Na_4P_2O_7$ species on the used catalysts is lower than that on the fresh catalyst, especially that of $Na_4P_2O_7$. It is presumed that the surface of the

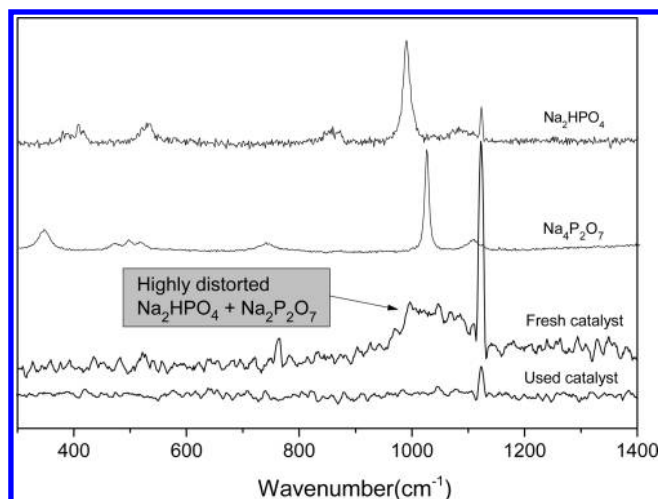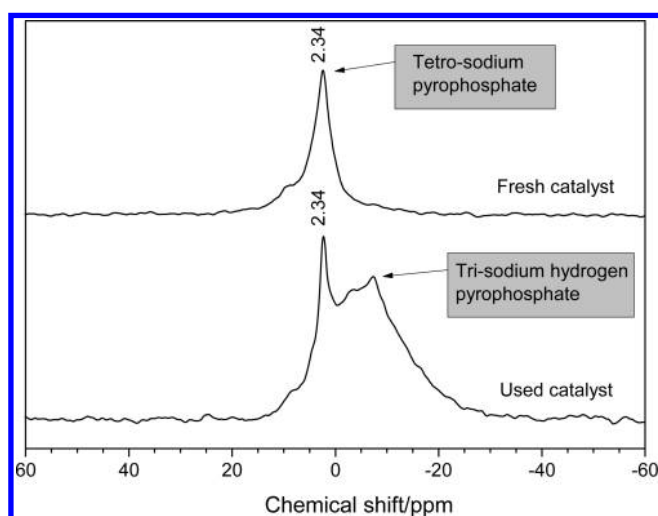used catalyst is covered by sodium lactate together with a certain amount of phosphate and poly lactate.

The ^{31}P MAS NMR technique was also used to investigate the fresh and used catalyst (Figure 13). Over the fresh catalyst, an intense peak at 2.3 ppm ascribable to $Na_4P_2O_7$ species is observed.[46] Over the used catalyst, additional peaks in the range of −20 to 0 ppm are detected. According to Gunter et al.,[40] the additional peaks can be ascribed to trisodium hydrogen pyrophosphate generated through proton exchange of sodium lactate. Therefore, the NMR investigation provided indirect evidence for the existence of sodium lactate species on the catalyst during the reaction.

Y zeolite has well developed and organized three-dimensional channels with 0.74 nm aperture, easy for access by small sized molecules such as LA, AA, and so forth, while difficult for diffusion by large sized molecules such as 2,3-pentanedione, poly lactate, and so forth. Thus NaY supported catalyst may suppress the formation of 2,3-pentanedione and poly lactate while enhance the production of AA. The results of the present study clearly demonstrated this point. On the other hand, previous

study[47] indicated that strong catalyst acidity is unfavorable for the target reaction (AA formation); therefore, the fully Na^+-exchanged NaY based catalyst can eliminate strong Brønsted acid sites to restrain side reactions (pyrolysis of LA and further reaction of AA).

As demonstrated early, Na_2HPO_4-modified NaY has lower acid strength than unmodified NaY. Strong acidity of catalyst accounts for lower AA yield[47] since it enhances the side reactions such as decarboxylation and/or decarbonylation of LA to acetaldehyde and CO_x and further reaction of AA. Therefore, acid strength plays an important role in determining the product distribution. Moreover, catalyst structure also shows certain effect on product distribution, especially on 2,3-pentanedione formation. Over Na_2HPO_4-modified NaY, small fraction of 2,3-pentanedione is formed likely because of the confinement effect in the narrowed micropores of NaY.

4. CONCLUDING REMARKS

In the present study we modified the fully Na^+-exchanged Y zeolite with alkali phosphates for the catalytic dehydration of LA to AA. The introduction of alkali phosphates can somehow modify the morphology of NaY crystallites. The loading of alkali phosphate can also have an effect on the pore structure and surface area of NaY. The NH_3-TPD results revealed that the addition of alkali phosphate caused notable decrease in surface acidity (in terms of both density and strength). The FTIR study of pyridine adsorption suggested that the introduction of alkali phosphate species does not create any extra acidity, and Brønsted acid sites are absent on the surface of the modified NaY. After tuning of parameters such as type and loading of alkali phosphate, reaction temperature, LHSV, and LA concentration in solution, an AA yield of 58.4% is achieved over the 14 wt % Na_2HPO_4/NaY catalyst. On the basis of the results of FTIR, Raman, and MAS ^{31}P NMR characterizations collected over the fresh and used catalysts, the excellent performance of 14 wt % Na_2HPO_4/NaY is related to (i) the existence of sodium lactate that is in situ generated via proton transfer on the NaY support, and (ii) the surface phosphate groups that can stabilize the carboxyl group of LA reactant and AA product. With time on stream, polymerization of lactate occurs on the catalyst surface, causing a decline of AA selectivity. The used catalyst can be reactivated through treatment in air at 500 °C. The reactivated catalyst shows 100% recovery in LA conversion as well as better performance in terms of lesser decline of AA selectivity with time.

■ AUTHOR INFORMATION

Corresponding Author

*W.-J.J.: Phone: +86-25-83686270. Fax: +86-25-83317761. E-mail: jiwj@nju.edu.cn. C.-T.A.: Phone: +852-34117067. Fax: +852-34117348. E-mail: pctau@hkbu.edu.hk.

■ REFERENCES

(1) Danner, H.; Dürms, M.; Gartner, M.; Braun, R. Appl. Biochem. Biotechnol. 1998, 70, 887–894.

(2) Xu, X. B.; Lin, J. P.; Cen, P. L. Chin. J. Chem. Eng. 2006, 14, 419–427.

(3) Lin, M. M. Appl. Catal., A 2001, 207, 1–16.

(4) Yang, X. J.; Feng, R. M.; Ji, W. J.; Au, C. T. J. Catal. 2008, 253, 57–65.

(5) Mizuno, N.; Tateishi, M.; Iwamoto, M. Appl. Catal., A 1995, 128, L165–L170.

(6) Ushikubo, T.; Nakamura, H.; Koyasu, Y.; Wajiki, S. U.S. Patent 5 380 933, 1995.

(7) Lin, M. M. Appl. Catal., A 2003, 250, 305–318.

(8) Botella, P.; Nieto, J. M. L.; Solsona, B.; Mifsud, A.; Marquez, F. J. Catal. 2002, 209, 445–455.

(9) Albonetti, S.; Cavani, F.; Trifiro, F. Catal. Rev. 1996, 38, 413–438.

(10) Jarvinen, M.; Myllykoski, L.; Keiski, R.; Sohlo, J. Bioseparation 2000, 9, 163–166.

(11) Timmer, J. M. K.; Kromkamp, J.; Robbertsen, T. J. Membr. Sci. 1994, 92, 185–197.

(12) Tejayadi, S.; Cheryan, M. Appl. Microbiol. Biotechnol. 1995, 43, 242–248.

(13) Fan, Y. X.; Zhou, C. H.; Zhu, X. H. Catal. Rev. 2009, 51, 293–324.

(14) Holmen, R. E. U.S. Patent 2 859 240, 1958.

(15) Paparizos, C.; Dolhyj, S. R.; Shaw, W. G. U.S. Patent 4 786 756, 1988.

(16) Sawicki, R. A. U.S. Patent 4 729 978, 1988.

(17) Gunter, G. C.; Miller, D. J.; Jackson, J. E. J. Catal. 1994, 148, 252–260.

(18) Gunter, G. C.; Langford, R. H.; Jackson, J. E.; Miller, D. J. Ind. Eng. Chem. Res. 1995, 34, 974–980.

(19) Wadley, D. C.; Tam, M. S.; Kokitkar, P. B.; Jackson, J. E.; Miller, D. J. J. Catal. 1997, 165, 162–171.

(20) Miller, D. J.; Jackson, J. E.; Langford, R. H.; Gunter, G. C.; Tam, M. S.; Kokitkar, P. B. U.S. Patent 731 471, 1998.

(21) Tam, M. S.; Gunter, G. C.; Craciun, R.; Miller, D. J.; Jackson, J. E. Ind. Eng. Chem. Res. 1997, 36, 3505–3512.

(22) Tam, M. S.; Craciun, R.; Miller, D. J.; Jackson, J. E. Ind. Eng. Chem. Res. 1998, 37, 2360–2366.

(23) Tam, M. S.; Jackson, J. E.; Miller, D. J. Ind. Eng. Chem. Res. 1999, 38, 3873–3877.

(24) Monma, H. J. Catal. 1982, 75, 200–203.

(25) Daniel, C. U.S. Patent 4 410 729, 1983.

(26) Watkins, W. C. U.S. Patent 3 917 673, 1975.

(27) Mok, W. S. L.; Antal, M. J., Jr.; Jones, M., Jr. J. Org. Chem. 1989, 54, 4596–4602.

(28) Lira, C. P.; McCrackin, P. J. Ind. Eng. Chem. Res. 1993, 32, 2608–2613.

(29) Fisher, C. H.; Rehberg, C. E.; Smith, L. T. J. Am. Chem. Soc. 1943, 65, 763–767.

(30) Rehberg, C. E.; Fisher, C. H. J. Am. Chem. Soc. 1944, 66, 1203–1207.

(31) Ratchford, W. P.; Fisher, C. H. Ind. Eng. Chem. 1945, 37, 382–387.

(32) Park, C.; Keane, M. A. J. Mol. Catal. A: Chem. 2001, 166, 303–322.

(33) Wells, R. P. K.; Tynjala, P.; Bailie, J. E.; Willock, D. J.; Watson, G. W.; King, F.; Rochester, C. H.; Bethell, D.; Page, P. C. B.; Hutchings, G. J. Appl. Catal., A 1999, 182, 75–84.

(34) Wang, H. J.; Yu, D. H.; Sun, P.; Yan, J.; Wang, Y.; Huang, H. Catal. Commun. 2008, 9, 1799–1803.

(35) Sun, P.; Yu, D. H.; Fu, K.; Gu, M.; Wang, Y.; Huang, H.; Ying, H. Catal. Commun. 2009, 10, 1345–1349.

(36) Zhang, Z. Q.; Qu, Y. X.; Wang, S.; Wang, J. D. Ind. Eng. Chem. Res. 2009, 48, 1119–1129.

(37) Zhang, J. F.; Lin, J. P.; Cen, P. Can. J. Chem. Eng. 2008, 86, 1047–1053.

(38) Busca, G. In Metal Oxides, Chemistry and applications; Fierro, J. L. G., Ed.; CRC-Taylor & Francis: Boca Raton, FL, 2006; p 247.

(39) Benaliouche, F.; Boucheffa, Y.; Ayrault, P.; Mignard, S.; Magnoux, P. Microporous Mesoporous Mater. 2008, 111, 80–88.

(40) Lercher, J. A. In Catalysis-an Integrated Approach; van Santen, R. A., van Leeuwen, P., Moulijn, J. A., Averill, B. A., Eds.; Elsevier: Amsterdam, The Netherlands, 1999; p 543.

(41) Rouquerol, J.; Llewellyn, P.; Rouquerol, F. In Studies in Surface Science and Catalysis 167: Characterization of Porous Solids VII;

Llewellyn, P. L., Rodriquez-Reinoso, F., Rouqerol, J., Seaton, N., Eds.; Elsevier: Amsterdam, The Netherlands, 2007; p 49.

(42) Jentys, A.; Lercher, J. A. In *Studies in Surface Science and Catalysis 137: Introduction to Zeolite Science and Practice*; van Bekkum, H.; Flanigen, E. M.; Jacobes, P. A.; Jansen, J. C., Eds.; Elsevier: Amsterdam, The Netherlands, 2001; p 454.

(43) Gunter, G. C.; Craciun, R.; Tam, M. S.; Jackson, J. E.; Miller, D. J. *J. Catal.* **1996,** *164*, 207–219.

(44) Smith, L. T.; Fisher, C. H.; Ratchford, W. P.; Fein, M. L. *Ind. Eng. Chem.* **1942,** *34*, 473–479.

(45) Li, G. H.; Larsen, S. C.; Grassian, V. H. *Catal. Lett.* **2005,** *103*, 23–32.

(46) Hayashi, S.; Hayamizu, K. *Bull. Chem. Soc. Jpn.* **1989,** *62*, 3061–3068.

(47) Balkus, K. J.; Khanmamedova, A. K. *J. Catal.* **1995,** *151*, 10–16.